Partial density of Mn 3d states and exchange-splitting changes in $Zn_{1-x}Mn_xY$ (Y=S,Se,Te)

R. Weidemann, H.-E. Gumlich, M. Kupsch, and H.-U. Middelmann
Fachbereich Physik, Technische Universität Berlin, Hardenbergstrasse 36, D-1000 Berlin 12, Germany

U. Becker
Fritz-Haber-Institut der Max-Planck-Gesellschaft, Faradayweg 4-6, D-1000 Berlin 33, Germany
(Received 25 June 1991)

Mn 3d states in $Zn_{1-x}Mn_xY$ (Y=S,Se,Te) have been investigated using resonant synchrotron-radiation photoemission at the Mn 3p-3d threshold. We observe chemical trends due to anion substitution for the main Mn 3d photoemission feature at 3.5, 3.6, and 3.8 eV below the valence-band maximum as well as for the $d(\uparrow)$-$d(\downarrow)$ exchange splitting for $Zn_{0.81}Mn_{0.19}S$, $Zn_{0.81}Mn_{0.19}Se$, and $Zn_{0.68}Mn_{0.32}Te$, respectively. The size of relaxation effects associated with the resonant-photoemission process is derived. Valence-band offsets of 0.3 eV are found between the semimagnetic Zn compounds and their parent binary alloys.

I. INTRODUCTION

Mn-doped II-VI semimagnetic semiconductors (SMSC's) have attracted considerable interest for several years.[1-4] Beside the well-known changes in the electronic structure of ordinary ternary semiconducting compounds due to the composition, II-VI compounds show in addition novel magneto-optical and magnetotransport properties if the cation is partly substituted by Mn with its half-filled 3d shell. In this context the interaction between Mn 3d electrons and the electronic states of the host crystal is of special interest. In recent photoemission studies the contribution of the Mn 3d states to the valence-band density of states (DOS) was investigated.[5-19] In recent years resonant-photoemission measurements[11-19] on $Cd_{1-x}Mn_xS$, $Cd_{1-x}Mn_xSe$, and $Cd_{1-x}Mn_xTe$ have resolved some controversies about the experimentally deduced partial Mn 3d DOS. Mn 3d-derived photoemission was found in the valence-band region from 0 to 10 eV below the valence-band maximum (E_v). At least three features were observed in all these alloys: a major Mn 3d structure at 3.3–3.8 eV below E_v (main structure), a weak structure at lower binding energy in the 0–2 eV range (valence structure), and a broad structure in the 6–9 eV range (satellite structure). Although the existence of these structures seems to be unquestionable by now, their interpretation as Mn 3d DOS or shakeup features and the conclusions to be drawn on their degree of hybridization with the anion p states are still quite controversial.

The variation in the relative intensities of these Mn 3d features by changing the anion in a compound series, like $Cd_{1-x}Mn_xY$ or $Zn_{1-x}Mn_xY$ (Y=S,Se,Te), is promising to clarify the amount of p-d hybridization in these alloys. Such a systematic study was reported for $Cd_{1-x}Mn_xY$,[11] but little work has been done on semimagnetic Zn compounds. Only one spectrum of $Zn_{1-x}Mn_xSe$ in Ref. 12 and of a $Zn_{1-x}Mn_xS$ film in Ref. 13 is available. In this paper we present, to our knowledge, the first systematic study of the Mn contribution to the valence band in $Zn_{1-x}Mn_xS$, $Zn_{1-x}Mn_xSe$, and $Zn_{1-x}Mn_xTe$. Our results show unexpected differences from the similar investigation on $Cd_{1-x}Mn_xY$ (Ref. 11) and lead to a model with a different degree of hybridization of the observed Mn 3d features.

We discuss our results according to recent theoretical calculations, mainly based on $Cd_{1-x}Mn_xTe$,[14,15,20-24] and by comparison with results for atomic Mn[25-27] we found clear evidence of satellite-photoemission structure in the partial Mn 3d DOS.

Assuming that the Zn 3d core level serves as a reference level for the alignment of the valence-band edges[28] we deduce the valence-band offsets (VBO's) between the ternary alloys and their parent binary compounds. We use this model also for estimating chemical trends from photoemission spectra.

II. EXPERIMENT

The photoemission experiments were performed at the Berlin storage ring BESSY using the toroidal grating monochromator TGM 7 for photon energies between 30 and 80 eV with a photon-energy resolution at the Al $2p_{3/2}$ edge of 0.16 eV. Angle-resolved energy distribution curves (EDC's) were measured with a vacuum science workshop (VSW) hemispherical analyzer (Model No. HA50), operated at 10 eV pass energy. The electrons were detected at normal emission with an overall energy resolution of 0.4 eV at a photon energy of 80 eV. The samples were illuminated with light from a standard halogen light source to prevent electrostatic charging.

Bulk single crystals of $Zn_{1-x}Mn_xY$ were grown at the material laboratory at the Technical University Berlin by a modified Bridgman method. In general we have used crystals with zinc-blende structure checked by x-ray diffraction, except $Zn_{1-x}Mn_xS$, which is hexagonal. The Mn concentration of the ternary compounds were measured by atomic absorption spectroscopy, resulting in

$x = 0.19$, 0.19, and 0.32 for $Zn_{1-x}Mn_xS$, $Zn_{1-x}Mn_xSe$, and $Zn_{1-x}Mn_xTe$, respectively. The samples were cleaved in the atmosphere before loading the preparation chamber with pieces having 6–10 mm^2 mirrorlike surfaces. We followed the cleaning procedure described in Refs. 29–32 for CdTe by Ar sputtering and annealing. In fact, the success of this procedure for Zn compounds has been checked by Auger electron spectroscopy, finding clean and stoichiometric surfaces. The prepared samples were transferred under ultra-high-vacuum conditions ($6\times10^{-11} < p < 4\times10^{-10}$ mbar) into the photoemission chamber, and the recorded photoemission spectra are very similar to EDC's obtained from *in situ* cleaved samples (Refs. 33 and 34), whereas EDC's from smooth surfaces clearly show an additional structure.

III. RESULTS AND DISCUSSION

General valence-band photoemission

EDC's for $Zn_{1-x}Mn_xY$ and for ZnY (Y=S,Se,Te) were taken at various photon energies between 40 and 60 eV. In Fig. 1 spectra are plotted for comparison of ternary and binary valence-band features for $Zn_{0.68}Mn_{0.32}Te$ and ZnTe [1(a)], $Zn_{0.81}Mn_{0.19}Se$ and ZnSe [1(b)], and $Zn_{0.81}Mn_{0.19}S$ and ZnS [1(c)]. The Mn-derived features are most pronounced at the Mn 3p-3d threshold near 50 eV and are discussed in the next section. The details of the valence-band structures of the binary compounds (lower curves) are poorly resolved in these spectra due to the short data acquisition time (~5 min/spectrum), but general agreement is given with the results of Ley *et al.*,[33] Eastman *et al.*,[34] and Shevshik *et al.*[35] The feature within the first 3 eV below E_v, which is best resolved for ZnS, reflects primarily anion-p character, and the feature between 3–6 eV below E_v, which is best resolved for ZnTe, reflects primarily metal-s character. Note the different scaling factors in the enlarged part of the spectra in Fig. 1, indicating an increasing cross section for the anion-p electrons as one goes from Te(5p) to Se(4p) to S(3p).

The position of the valence energy E_v is determined by a linear extrapolation of the leading edge of the valence band, resulting in different positions of E_v for the ternary and binary alloys, respectively. This displacement leads to different binding energies for the Zn 3d level, which are summarized in Table I. However, as indicated in Fig. 1 we have ascribed this displacement to a shift of the valence-band edges of the ternary alloys. A shift of the Zn 3d level with composition is not expected due to the nearly constant Zn-anion binding distances[36,37] in the ternary alloys. This reasoning was supported by a photoemission study of the electronic structure of $Cd_{1-x}Mn_xS$. Wall *et al.*[16] found no detectable shift of the Cd 4d level between the ternary and binary compounds with respect to the Fermi level.[38] The authors also observed a difference in the valence-band edges of 0.31(16) eV but do not ascribe this shift to a change in the ternary DOS. Such a change in the valence-band DOS on the other hand, was observed on Fe-based SMSC's. Very recently Denecke *et al.*[39] reported for $Cd_{1-x}Fe_xSe$ and CdSe a clear shift of about 1 eV between the valence-band edges of the ternary and binary compounds. Taking into account all observations available at present we conclude that the shift of the valence-band edges is due to the interaction of the Mn 3d levels with the anion-p levels. Since the p-d interaction is repulsive,[40] the reduced energetic separation between the anion-p and Mn d states of 3–4 eV, which is compared to the value of 9–10 eV be-

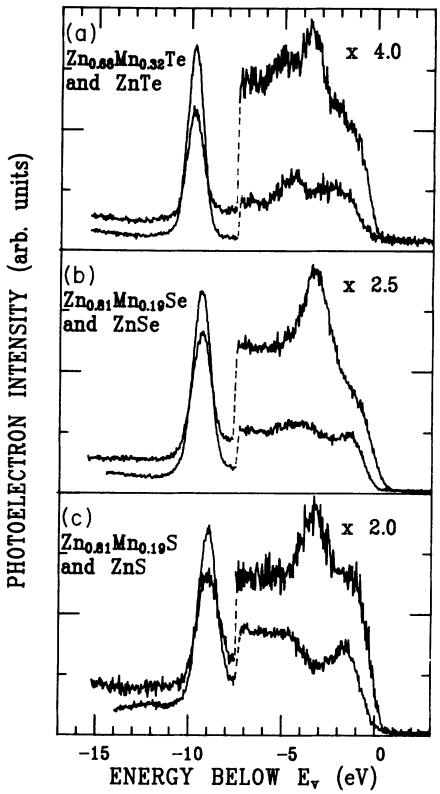

FIG. 1. EDC's for (a) $Zn_{0.68}Mn_{0.32}Te$ and ZnTe, (b) $Zn_{0.81}Mn_{0.19}Se$ and ZnSe, and (c) $Zn_{0.81}Mn_{0.19}S$ and ZnS taken at 50 eV photon energy. The pairs of spectra have been normalized to the integrated Zn 3d intensity scaled by the Zn concentration ($1-x$). The lower part of the spectra are plotted in enlarged scales, and the energy scale is related to the valence-band edges of the binary compounds.

TABLE I. Binding energies of the Zn 3d core level in semimagnetic $Zn_{1-x}Mn_xY$ (Y=S,Se,Te). The difference between the ternary and their parent binary compounds corresponds to their natural valence-band offsets.

	$E_{Zn\,3d}$ (eV)	Difference (eV)
$Zn_{0.81}Mn_{0.19}S$	9.33(6)	0.36(12)
ZnS	8.97(6)	
ZnS[a]	9.03(15)	
$Zn_{0.81}Mn_{0.19}Se$	9.62(7)	0.25(14)
ZnSe	9.37(7)	
ZnSe[a]	9.20(15)	
$Zn_{0.68}Mn_{0.32}Te$	10.06(10)	0.26(25)
ZnTe	9.80(15)	
ZnTe[a]	9.84(15)	

[a]Reference 33.

tween anion-p and Zn d states, will move the anion-p states to a lower binding energy. This interpretation is consistent with the sign and the order of magnitude of the VBO's of these semiconductors if interface-specific dipole effects are assumed to be negligible.[41] To our knowledge photoemission experimental data of VBO's in semimagnetic $Zn_{1-x}Mn_xY/ZnY$ have not been published so far. However, in a heterojunction study on ZnSe:MnSe:ZnSe by Asonen *et al.*[42] a VBO of 0.16(5) eV was observed by photoemission spectroscopy, which is in agreement with the value for $Zn_{0.81}Mn_{0.19}Se/ZnSe$ determined in our present study (Table I).

Resonant photoemission and Mn 3*d* contribution

We have investigated the Mn contribution in the valence-band region by use of resonant-photoemission spectroscopy at the Mn 3*p*-3*d* threshold. At resonance a Mn 3*p* electron is excited into the empty part of the Mn 3*d* states. This excited state can decay *via* autoionization, at which a 3*d* electron drops down to fill the 3*p* hole, transferring energy to another 3*d* electron that is ejected into the continuum [Eq. (1)]. The final state is indistinguishable from the state reached by direct photoemission [Eq. (2)], and the interference between the two channels is characterized by the Fano line shape (3) for the photoemission intensity as the photon energy is swept through the 3*p*-3*d* threshold. In formula (3) E_R is the resonance energy, Γ the full width at half maximum (FWHM), q Fano's asymmetry parameter, and I_0 the nonresonant Mn 3*d* emission:

$$3p^6d^5+h\nu\rightarrow 3p^5d^6\rightarrow 3p^6d^4\varepsilon_f\ , \tag{1}$$

$$3p^6d^5+h\nu\rightarrow 3p^6d^4\varepsilon_f\ , \tag{2}$$

$$I(h\nu)=I_0\frac{(\varepsilon+q)^2}{1+\varepsilon^2},\quad \varepsilon=\frac{E_R-h\nu}{\Gamma/2}\ . \tag{3}$$

The resonant enhancement of the Mn 3*d* states in the valence band of $Zn_{0.68}Mn_{0.32}Te$ is visible in Fig. 2, which shows constant initial-state (CIS) spectra for selected initial-state energies. By comparison with the absorption spectrum of atomic Mn, which is plotted in the lower part of Fig. 2, the dominant feature is attributed to the Mn $3p^53d^6\,{}^6P$ final state. The shift of the ^6P excitation relative to the atomic absorption is discussed by considering chemical trends, see below. Deviations from the fitted Fano line shapes (solid lines) for each spectrum occur at the high-energy side of the ^6P excitation at photon energies between 51 and 54 eV. Auger emission may contribute to this part of the spectra, and photoemission from excited or ionized Mn shows structures in this part as well.[25] Other multiplets of the final-state configuration (^6F,^6D) as well as excitation of the Mn $3p^53d^54s^2\ nl$ Rydberg series may produce additional structures in the CIS spectra. A detailed analysis of the Fano parameter in formula (3) is complicated by the strong correlation of the fitting parameters.[43] This problem originates from the noninterfering background emission, which in principle depends on the photon energy and has to be added to

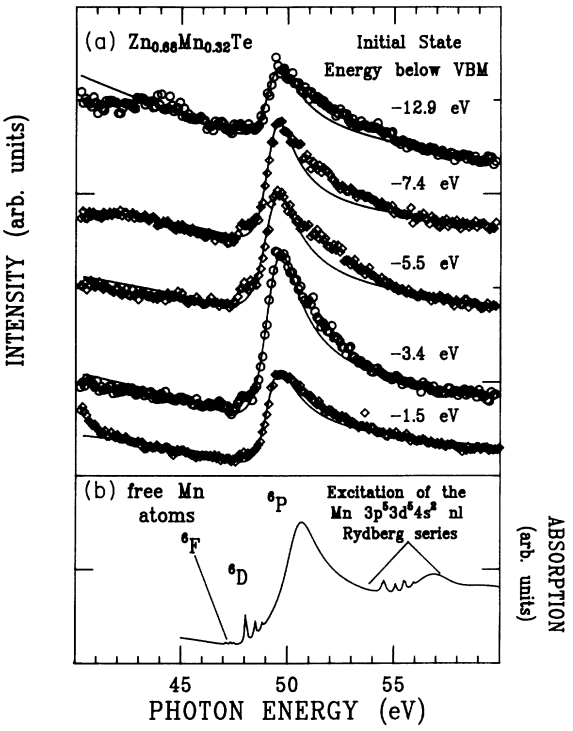

FIG. 2. (a) Constant initial-state (CIS) spectra of selected valence-band regions that are identified by their initial or binding energy E_i. The solid line is a fit to formula (3) with parameters given in Table II. (b) The absorption spectrum of free Mn atoms is adopted from Ref. 27.

formula (3). To avoid this problem Ley *et al.*[14] have fixed the position E_R and width Γ during the fit. Wall *et al.*[16] have analyzed the ratio of CIS spectra, which they have calculated from CIS spectra for the ternary and binary semiconductor at a given initial-state energy. In contrast to those authors we have generated CIS-type spectra by measuring the peak area above the inelastic background at a given binding energy directly from the EDC's. In doing this we have extended the two established methods to obtain the partial density of Mn 3*d* states in the valence-band region of SMSC's. One method uses difference curves between ternary and binary materials[7,12] (*T-B*), and the other one uses difference curves between spectra taken at the Mn 3*p*-3*d* resonance ($h\nu\sim 50$ eV) and antiresonance ($h\nu\sim 47.5$ eV) positions (*R-AR*).[14,17] In Fig. 3 the *R-AR* difference curve for $Zn_{0.68}Mn_{0.32}Te$ is shown together with a fit of 3 Gaussian line shapes to the Mn-derived structures. Although the dotted-dashed background in Fig. 3 is only a simple approximation, it describes the background of a difference curve of two EDC's reasonably well. In fact, choosing a more smooth approximation for the background has little effect on the relative intensities of the Gaussian curves. To get CIS-type spectra of the Mn-derived structures we have performed this fitting procedure also for difference curves between spectra recorded at various photon energies and for the spectrum at the antiresonance position, respectively. The fitted areas of the Gaussian line shape were used to trace the photoemission cross section. A

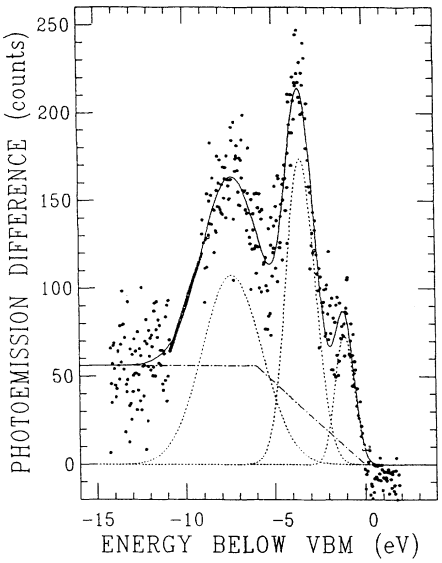

FIG. 3. Data reduction of the resonance-antiresonance difference curve for $Zn_{0.68}Mn_{0.32}Te$. The remaining Zn 3*d* structure between 8.5 and 11.0 eV is substituted by a linear approximation. The dotted-dashed line represents the Mn 3*d*–induced background emission, which models the partial Mn 3*d* DOS together with the three dashed Gaussian line shapes. For parameters see Table III.

careful normalization of the recorded EDC's before subtraction is necessary when using these methods. We choose the Zn 3*d* emission as a reference for intensity normalization as well as for binding-energy calibration because of its constant photoemission cross section[44] and the weak dispersion[45] of the Zn 3*d* emission. The resulting CIS-type spectra of the Mn 3*d* features for $Zn_{0.68}Mn_{0.32}Te$ are shown in Fig. 4. The photon-energy-dependent cross section of the main structure near the Mn 3*p*-3*d* threshold exhibits a Fano-resonance behavior, which is well described by the Fano line shape (3) with a small uncertainty in the values of the fitting parameter in Table II. Using these values as start values for a fit of a Fano line shape to the normal CIS spectra in Fig. 2, we obtain a satisfactory agreement with the experimental data. Comparing the parameter in Table II, a weak trend of the asymmetry parameter q from 2.4 to 1.8 is found if the initial-state energy E_i changed from 5.5 to 1.5 eV below E_v. Since a Fano line shape with reduced q value shows a more pronounced dip at photon energies just below the resonance maximum (antiresonance), the trend of q may be explained by an increase of *p-d* hybridization for Mn 3*d* states nearby the valence-band maximum. Because in transition-metal compounds the d^{n-1} atomiclike final state tends to exhibit Fano-like resonances, whereas d^nL final states that correspond to hybridized states show a more pronounced antiresonance behavior.[46] L denotes a ligand hole as results of charge transfer screening of the hole of the initial Mn 3*d* excitation.

Returning to Fig. 4 we found that the cross section of the satellite structure is not described by a single Fano line shape but shows a second maximum near 56 eV photon energy, which is not resolved in the normal CIS spectra of Fig. 2. This new feature in the CIS-type spectra of the satellite structure can be used to clarify the origin of this structure in the partial Mn 3*d* DOS. A secondary rise near 56 eV is also observed in the partial cross section for the Mn 3*d* satellite photoemission of Mn vapor,[26] which is plotted in Fig. 4(b). The similar behavior of the atomic cross section with the CIS-type spectra of the compound satellite structure is a fingerprint of two-electron transitions and proves that the satellite structure is indeed associated with atomiclike satellite photoemission.

In the previous sections results for $Zn_{0.68}Mn_{0.32}Te$ have been predominantly discussed, because the satellite structure is most intensive in this alloy. However, the results hold also for $Zn_{0.81}Mn_{0.19}Se$ and $Zn_{0.81}Mn_{0.19}S$. Following we stress the common features of the partial Mn 3*d* DOS before we discuss the differences due to the change of hybridization in the anion series Te, Se, S.

In Figs. 5(a)–5(c) we show the partial density of Mn 3*d* states for $Zn_{0.68}Mn_{0.32}Te$, $Zn_{0.81}Mn_{0.19}Se$, and $Zn_{0.81}Mn_{0.19}S$, respectively, obtained with both the *T-B* difference method (upper curves) and with the *R-AR* difference method (lower curves). The Mn 3*d* contribution in Figs. 5(a)–5(c) shows three features in all cases: a dominant main structure at 3.5–3.8 eV below E_v, a weak valence structure at lower binding energies in the 0–2 eV range, and a broad satellite structure in the 6–9 eV

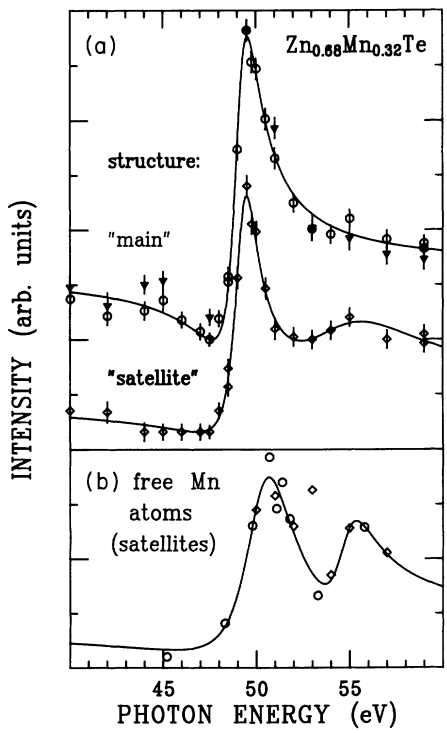

FIG. 4. (a) Partial cross section of the Mn 3*d* main and satellite structures for $Zn_{0.68}Mn_{0.32}Te$. The symbols are deduced from resonance-antiresonance difference curves (circles and diamonds) and ternary-binary difference curves (triangles). (b) Partial cross section of the Mn 3*d* photoelectron satellite lines for free Mn atoms (Ref. 26). The lines are a guide to the eye; for the main structure see also Fig. 7.

TABLE II. Parameters obtained by fitting the Fano line shape (3) to the CIS spectra of $Zn_{0.68}Mn_{0.32}Te$ in Fig. 2, together with the results for $Zn_{0.81}Mn_{0.19}Se$ and $Zn_{0.81}Mn_{0.19}S$. The initial states are identified by their binding energy E_B. The results of the CIS-type spectra for the main Mn 3*d* structure are listed together with the values of the CIS spectra for $E_B = 3.4$ eV (second line), the position of the main structure. The errors given (in parentheses) correspond to three times the rms values.

	$Zn_{0.68}Mn_{0.32}Te$				$Zn_{0.81}Mn_{0.19}Se$				$Zn_{0.81}Mn_{0.19}S$			
E_B (eV)	E_R (eV)	Γ (eV)	q	I_0	E_R (eV)	Γ (eV)	q	I_0	E_R (eV)	Γ (eV)	q	I_0
12.9	49.5(1)	1.7(3)	2.3(2)	0.4	49.6(2)	1.5(4)	2.2(3)	0.3	49.9(1)	2.3(2)	2.4(1)	0.4
7.4	49.5(1)	1.6(1)	2.2(2)	0.7	49.6(1)	1.3(2)	2.0(2)	0.6	49.7(1)	1.3(2)	2.1(2)	0.8
5.5	49.4(1)	1.9(2)	2.4(2)	0.6	49.6(1)	1.5(2)	2.6(2)	0.4	49.7(1)	1.6(2)	2.6(2)	0.6
3.4	49.5(1)	1.9(2)	2.2(1)	1.0	49.6(1)	1.6(2)	2.2(1)	1.0	49.8(1)	1.9(2)	2.3(1)	1.0
	49.33(7)	1.6(2)	1.85(7)		49.56(6)	1.6(1)	2.0(1)		49.77(6)	1.8(2)	2.15(6)	
1.5	49.4(1)	1.6(2)	1.8(1)	0.8	49.6(1)	1.6(2)	1.8(1)	0.6				

range. The results of both methods are generally consistent with each other, however slight differences between the *R-AR* and *T-B* curves occur near 5 eV. In Fig. 5(b) this difference is due to Se 3*d* core-level emission originating from second-order light. The difference in Fig. 5(c) is due to a small displacement of the DOS feature with predominantly metal character in ZnTe and $Zn_{0.68}Mn_{0.32}Te$, respectively [see Fig. 1(a)]. Only two of the six spectra in Fig. 5 are affected, namely the *R-AR* curve in Fig. 5(b) and the *T-B* curve in Fig. 5(c). Although these effects are small, we have included corrections for the above-mentioned effects in our data-reduction procedure.

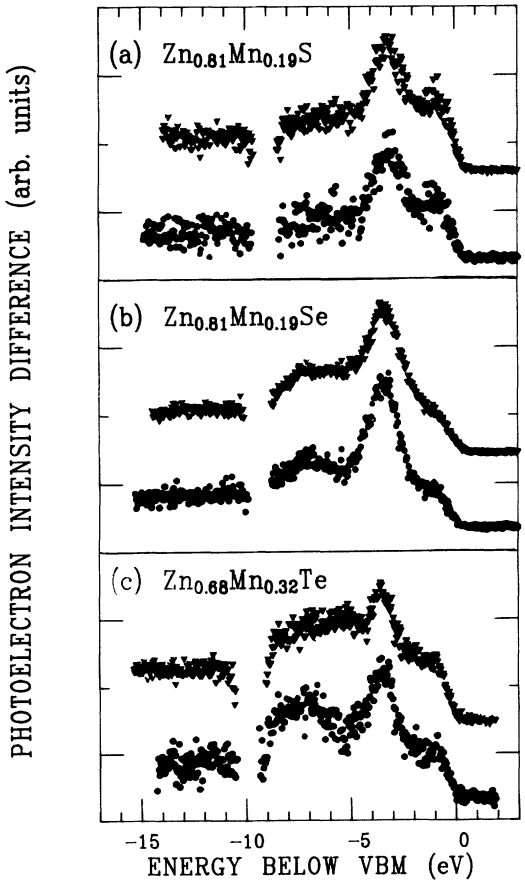

FIG. 5. Partial density of Mn 3*d* states in the valence-band region of (a) $Zn_{0.81}Mn_{0.19}S$, (b) $Zn_{0.81}Mn_{0.19}Se$, and (c) $Zn_{0.68}Mn_{0.32}Te$ obtained with the ternary-binary difference method (triangles) and resonance-antiresonance method (circles). The energy scale is related to the VBM of the binary alloys.

Electronic structure calculations are available for $Cd_{1-x}Mn_xTe$ (Refs. 20–24) and were also used to interpret the Mn-derived structures of other Mn-substituted II-VI SMSC's. In the tetrahedral crystal field the Mn 3*d* states split into states with $\Gamma_{12}(e)$ and $\Gamma_{15}(t_2)$ symmetry, respectively, where the $3d(t_2)$ state hybridizes with the anion *p* states of equal symmetry and the Mn $3d(e)$ state remains localized because of the absence of anion states with equal symmetry. The main peak in the overall structure of the partial density of Mn 3*d* states is only weakly influenced by the change of hybridization in the anion series Te-Se-S, which hints at the existence of localized states. Consequently we attribute this feature to the Mn $3d(e)$ initial states. The valence structure presumably originates *via* emission from the hybridized $\Gamma_{15}(t_2)$ states, whereas the satellite structure seems not to be related to the partial density of Mn *d* states. Instead, the satellite structure represents a shake-up-like satellite of the main Mn 3*d* feature, which is not taken into account in the one-electron picture.

The electronic structure determined by calculation with an effective one-electron Hamiltonian shows agreement with the experimental data within the first 5 eV below the valence-band maximum (VBM), if the theoretical Mn 3*d* DOS feature with *e* symmetry is shifted about 1 eV to a higher binding energy.[21] A more recent calculation on antiferromagnetic zinc-blende MnTe (Ref. 15) gives direct satisfactory agreement with the experimentally observed density of Mn 3*d* states in $Cd_{1-x}Mn_xTe$, if the Mn ground state is $(d^5_\uparrow)(s_\uparrow)(p_\uparrow)$ rather than $(d^5_\uparrow)s^2$. There is not, in all cases, agreement in the interpretation of the Mn-derived features in $Cd_{1-x}Mn_xTe$. Taniguchi *et al.*[11,17] and Ley *et al.*[14] have interpreted their data with a semiempirical configuration-interaction calculation on a model cluster $MnTe^{6-}$ and have concluded, in contrast to Franciosi *et al.*,[15] that the main and valence-structure features are due to Mn $3d^4$–anion-*p* hybridization. These features have d^5L final states, whereas, on the other hand, the satellite structure is due to unscreened d^4 atomiclike final states. These calculations predict similar degrees of hybridization in the main and valence structures. However, on the basis of our results

different degrees of hybridization are more likely. This conflict may result from the purely ionic cluster configuration, where a possible delocalization of the ligand hole is not included.

Chemical trends

Chemical trends in the partial Mn 3d DOS due to anion substitution in the series $Zn_{1-x}Mn_xY$ (Y=Te,Se,S) are governed by the change of the Mn-anion bond lengths. Because of the nearly constant cation-anion bond lengths in the individual alloys, which has been shown by extended x-ray-absorption fine-structure (EXAFS) studies,[36,37] a Mn composition dependence is not expected in the alloy series.

From Fig. 5 we found that the binding energy of the main structure is 3.8, 3.7–3.5, and 3.5 eV for $Zn_{0.68}Mn_{0.32}Te$, $Zn_{0.81}Mn_{0.19}Se$, and $Zn_{0.81}Mn_{0.19}S$, respectively, showing a weak trend toward lower binding energies as we move up in the Periodic Table. The uncertainty of the value for $Zn_{0.81}Mn_{0.19}Se$ results from different values obtained with the *R-AR* and *T-B* methods; see Table III. This trend shows that the shift of E_v due to the deeper anion potential seen by the outer valence p electrons is not totally compensated by the shift of the Mn 3d states due to the more ionic character of the alloys. For all samples the FWHM of the main structure is 2 eV. The positions and the FWHM of the valence and satellite structures show no significant trends; but we deduced more information from the intensities of the valence and satellite structures relative to the main structure by considering the branching-ratios (BR's) of the two structures.

In Fig. 6 the BR's are plotted against V_{pd}, a parameter describing the amount of Mn 3d–anion-p hybridization. The values of V_{pd} are estimated by Larson *et al.*[22] and consistent with scaling theory.[47] Our results on $Zn_{1-x}Mn_xY$ show increasing BR's going from S to Te for the satellite structure. However, for the valence structure we find a minimum BR value for $Zn_{0.81}Mn_{0.19}Se$. In contrast, Taniguchi *et al.*[11] found a decreasing valence-structure intensity together with an increasing satellite-structure intensity going from S to Te for $Cd_{1-x}Mn_xY$. They used the BR's to adjust parameters in their semiempirical configuration-interaction calculation, which in turn predicts the increasing satellite emission associated with an reduced valence emission for the anion series S-Se-Te.

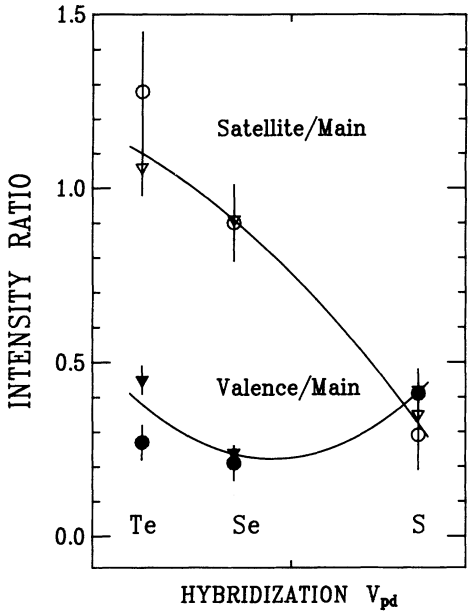

FIG. 6. Branching ratios of the valence structure (solid circles) and satellite structure (open circles) relative to the main structure are calculated from the areas under the Gaussian line shapes fitted to the difference curves of Fig. 5. Circles are deduced from the resonance-antiresonance curves and triangles are deduced from the ternary-binary curves of Fig. 5. The lines are a guide to the eye. The values of the hybridization parameter V_{pd} are adopted from Ref. 22.

The partial cross sections of the main structure, plotted in Figs. 7(a)–7(c), show a different trend. The resonance photon energy E_R of the main structure decreases from 49.77 to 49.33 eV going from S to Te. We note that the resonance energy of atomic Mn is 50.0 eV.[27] The trend of E_R is therefore in conflict with a changing hybridization due to anion substitution, because the material with the strongest hybridization $Zn_{0.81}Mn_{0.19}S$ has a value of E_R that is close to the value in the atomic case. To this end we have ascribed the shift of E_R to the unoccupied Mn 3d(↓) states. Referring to Eq. (1), E_R corresponds to the transition from the Mn 3p level to the empty Mn 3d(↓) states, which are split in the same manner as Mn 3d(↑)

TABLE III. Parameters obtained by fitting three Gaussian line shapes to the difference curves of Fig. 5. The positions E are given relative to the VBM in the binding energies, and Γ is the FWHM of the line shapes. The Gaussian line shapes represent the main, valence (val), and satellite (sat) features of the Mn 3d emission. *T-B* and *R-AR* denote difference curves obtained by the ternary-binary and resonance-antiresonance methods, respectively. The errors given (in parentheses) correspond to three times the rms values.

	Method	E_{main} (eV)	Γ_{main} (eV)	E_{val} (eV)	Γ_{val} (eV)	E_{sat} (eV)	Γ_{sat} (eV)
$Zn_{0.81}Mn_{0.19}S$	*T-B*	3.5(1)	2.1(3)	1.2(1)	1.3(1)	6.5(9)	3.8(2.1)
$Zn_{0.81}Mn_{0.19}Se$	*T-B*	3.5(1)	2.0(2)	1.3(2)	1.6(2)	6.5(3)	4.5(6)
$Zn_{0.68}Mn_{0.32}Te$	*T-B*	3.8(1)	2.0(2)	1.5(2)	1.5(3)	7.0(3)	4.3(7)
$Zn_{0.81}Mn_{0.19}S$	*R-AR*	3.5(1)	2.0(5)	1.2(2)	1.3(1)	6.5(9)	2.8(2.1)
$Zn_{0.81}Mn_{0.19}Se$	*R-AR*	3.7(1)	1.9(3)	1.3(2)	1.3(3)	6.8(5)	5.0(1.3)
$Zn_{0.68}Mn_{0.32}Te$	*R-AR*	3.8(1)	1.9(4)	1.4(3)	1.2(4)	7.6(3)	3.9(9)

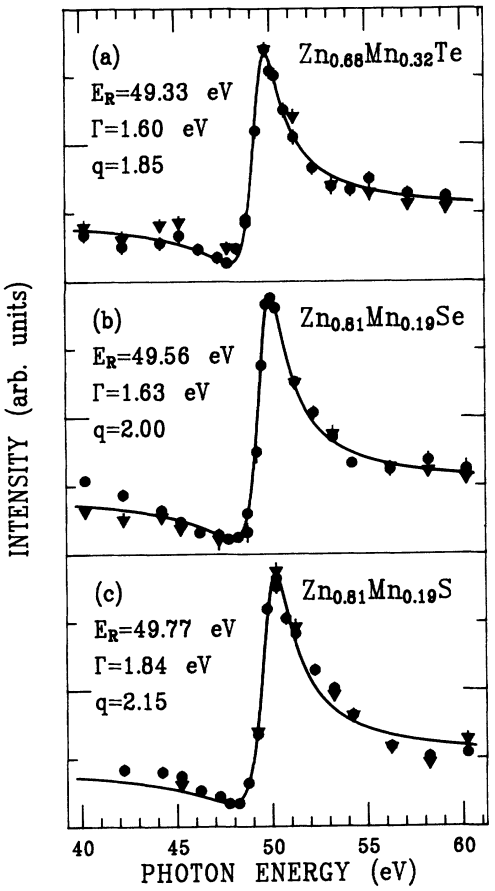

FIG. 7. Partial cross section of the main Mn $3d$ emission from (a) $Zn_{0.68}Mn_{0.32}Te$, (b) $Zn_{0.81}Mn_{0.19}Se$, and (c) $Zn_{0.81}Mn_{0.19}S$. The points are deduced from resonance-antiresonance difference curves (circles) and ternary-binary difference curves (triangles). The solid line represents a fit to Fano's formula (3).

states. The shift of E_R originates either in a shifted Mn $3p$ core level or, more likely, in a shift of the Mn $3d(\downarrow)$ states. Because the $3p$ photoline has a very low partial cross section, our experiments did not focus on determining the Mn $3p$ binding energy E_B. Thus, we only have an experimental Mn $3p$ E_B value for a $Zn_{1-x}Mn_xSe$ film on ZnS with $x \sim 0.3$: $E(\text{Mn } 3p) = 47.5$ eV,[13] which is close to the value observed for $Hg_{0.85}Mn_{0.15}Se$ (47.6 eV) by Franciosi *et al.*[18]

In order to find possible chemical trends in the $Zn_{1-x}Mn_xY$ series we are assuming that the Zn $3d$ core level serves as a reference level for all ternary alloys being studied in this work. Since many effects, such as surface shifts, are ignored in this model, it is somewhat surprising that our conclusions are in good agreement with theoretical predictions. The resulting energy-level scheme of the binary and ternary compounds are plotted with solid and dashed lines, respectively, in Fig. 8. The solid line arrows indicate experimental data taken to substantiate this model, whereas the dashed arrows are used for VBO's and the positions of the unoccupied $3d(\downarrow)$ states deduced from the model.

The VBO's between ZnS and ZnSe, ΔE_v(S,Se), and between ZnSe and ZnTe, ΔE_v(Se,Te), are 0.4 eV in each case. This value is in reasonable agreement with the results of Harrison[47] [ΔE_v(S,Se)=0.8 eV, ΔE_v(Se,Te)=1.1 eV], Langer and Heinrich[28] [ΔE_v(S,Se)=0.6 eV], and van der Walle[48] [ΔE_v(S,Se)=0.9 eV, ΔE_v(Se,Te)=1.4 eV].

The position of the unoccupied Mn $3d(\downarrow)$ states while a $3p$ hole is present is situated in the band gap for all ternary alloys that have been studied. However, to compare this position with the position of the unoccupied $3d$ state without an additional $3p$ hole, relaxation effects must be taken into account. Relaxation will shift the binding energies to higher values with respect to the unaffected ground state. A rough value of the relaxation energy may be derived from our measurements, but an inverse photoemission experiment is required to derive precisely the relaxation energy. Considering these restrictions of our model, the quasi-exchange-energy E_{ex}^* deduced from Fig. 8 is a lower limit of the exchange energy E_{ex}. Since cation substitution from Zn to Cd should not affect the exchange energy, we estimate the relaxation energy (E_{rel}) from Table IV, where values of E_{ex} from recent investigations are summarized. E_{ex} is defined as the difference between the ionization energy required to remove a d electron from the Mn $3d^5\,^6S$ ground state and the electron

TABLE IV. Exchange splitting E_{ex} between the Mn $3d$ states with spin up and down for $K_{1-x}Mn_xY$ (Y=Te,Se,S) with K=Zn,Cd. The change from Zn to Cd compounds should not effect E_{ex} because of the localized character of the relevant Mn $3d$ states. UPS+BIS denotes ultraviolet photoelectron spectroscopy combined with bremsstrahlung isochromat spectroscopy. XAS denotes x-ray absorption spectroscopy, where the position of the Mn $3d(\downarrow)$ states was deduced from a XAS line-shape analysis.

	E_{ex}^* (eV)	E_{ex} (eV)	E_{ex} (eV)	E_{ex} (eV)	E_{ex} (eV)
$K_{1-x}Mn_xTe$	5.1	8.4	6.8	7.0	7.7
$K_{1-x}Mn_xSe$	5.7			7.6	
$K_{1-x}Mn_xS$	6.0			7.9	9.2
Method	Fig. 8	UPS+BIS	XAS	Theory	Theory
Source	a	b	c	d	e

[a]This work.
[b]Reference 15.
[c]Reference 50.
[d]Reference 22.
[e]Reference 51.

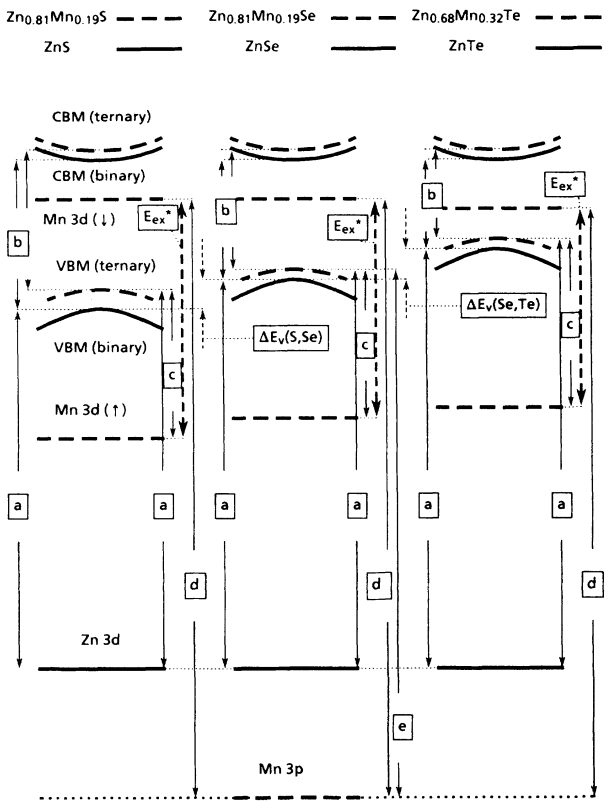

FIG. 8. Energy-level scheme for the ternary and binary compounds studied in which the Zn 3*d* levels is at fixed energy for all compounds. The energies used in this scheme are (a) the binding energies of the Zn 3*d* levels from Table I; (b) the band gaps are from reflectivity measurements (Ref. 49) obtained on the same samples used in this study at room temperature: 3.74 eV for ZnS, 3.61 eV for $Zn_{0.81}Mn_{0.19}S$, 2.68 eV for ZnSe, 2.68 eV for $Zn_{0.81}Mn_{0.19}Se$, 2.25 eV for ZnTe, and 2.42 eV for $Zn_{0.68}Mn_{0.32}Te$; (c) the binding energies of the main-structure from Table III; (d) the resonance energies E_R from Fig. 7; (e) the Mn 3*p* binding energy (47.5 eV) for $Zn_{1-x}Mn_xSe$, see text. From this scheme we deduce the exchange splittings E_{ex}^* between the Mn 3*d*(↑) and (↓) states in presence of a 3*p* hole. The values for E_{ex}^* are summarized in Table IV and were used in turn to derive approximate relaxation energies (see text).

affinity to add a *d* electron to the ground-state configuration. Thus, a combined photoemission and inverse photoemission experiment delivers directly the value of E_{ex}. However, although the exchange-splitting values being derived from ultraviolet photoemission spectroscopy (UPS) and bremsstrahlung isochromat spectroscopy (BIS) experiments are more realistic, the appearance of satellite photoemission also suggests that those values will be most likely an approximation. Using the (UPS+BIS) value of Table IV, we estimate $E_{rel}=E_{ex}-E_{ex}^*\sim 3$ eV. We note that a relaxation of this magnitude does move the position of the Mn 3*d*(↓) states without an additional 3*p* hole well above the conduction-band minimum for all alloys being studied in this work. Nevertheless, the relative chemical trend of E_{ex}^* due to anion substitution is in excellent agreement with the trend being derived from the reduction of screening as one goes from Te to Se to S.[22]

IV. CONCLUDING REMARKS

We have examined the Mn 3*d* contribution to the valence-band states of $Zn_{1-x}Mn_xY$ (Y=S,Se,Te). The partial density of Mn 3*d* states of the individual alloys is consistent with the results for $Cd_{1-x}Mn_xY$,[11] whereas the results in connection with anion substitution show unexpected differences to $Cd_{1-x}Mn_xY$. Our results support different amounts of hybridization for the Mn-derived structures: The valence structure exhibits the highest degree of hybridization with the anion-*p* states; the main structure exhibits comparatively low hybridization, and the satellite structure is found to be a shake-up feature of the main-structure localized at the Mn atom.

The chemical trend supports an increase of d^5L final-state charge transfer going from Te to Se to S; however, the unexpected behavior of the intensity ratio of the valence structure, which exhibits a minimum intensity ratio for $Zn_{1-x}Mn_xSe$, should stimulate further experimental and theoretical work. The partial Mn 3*d* DOS should not depend on composition x. However, a growth of the valence-structure intensity relative to the main Mn 3*d* feature with x could explain the observed behavior, because our $Zn_{1-x}Mn_xTe$ ($x=0.32$) sample has a higher Mn composition as does our $Zn_{1-x}Mn_xSe$ and $Zn_{1-x}Mn_xS$ ($x=0.19$) samples. In a recent study on $Cd_{1-x}Mn_xTe$ an x dependence of the intensity ratio of the satellite structure was reported.[52] The degree of delocalization of the ligand hole L, which is sensitive to the band structure of each compound may also be important.

ACKNOWLEDGMENTS

We are indebted to A. Krost and H.-J. Broschat for growing the crystals. We wish to thank P. Marsiske and U. Pohl for performing x-ray diffraction and atomic absorption spectroscopy analyses. We are grateful to A. Wall and A. Franciosi for providing us with results of their work prior to publication. We gratefully acknowledge B. Burmester, Th. Kleemann, and Th. Kreitler for assistance in the photoemission measurements as well as J. Allman and W. B. Peatman for a critical reading of the manuscript. This work was supported by the Bundesministerium für Forschung und Technologie under Grant No. BMFT 05314CI and special funds of the Technische Universität Berlin (IFP 4/1).

[1] J. K. Furdyna, J. Appl. Phys. **53**, 7637 (1982).
[2] N. B. Brandt and V. V. Moshchalkov, Adv. Phys. **33**, 193 (1984).
[3] O. Goede and W. Heimbrodt, Phys. Status Solidi B **146**, 11 (1988).
[4] A. Franciosi, in *Diluted Magnetic (Semimagnetic) Semiconductors*, edited by R. L. Aggarwal, J. K. Furdyna, and S. von Molnar, MRS Symposia Proceedings No. 89 (Material

Research Society, Pittsburgh, 1987), p. 175.
[5]B. A. Orlowski, Phys. Status Solidi B **95**, K31 (1979).
[6]C. Webb, M. Kaminska, M. Lichtensteiger, and J. Lagowski, Solid State Commun. **40**, 609 (1981).
[7]E. Sobczak and H. Sommer, Phys. Status Solidi B **112**, K43 (1982).
[8]W. Zahorowski and E. Gilberg, Solid State Commun. **52**, 921 (1984).
[9]B. Velicky, J. Marek, G. Paolucci, V. Chab, M. Surman, and K. C. Prince, Festkoerperprobleme **XXV**, 247 (1985).
[10]V. Chab, G. Paolucci, K. C. Prince, M. Surman, and A. M. Bradshaw, Phys. Rev. B **38**, 12 353 (1988).
[11]M. Taniguchi, M. Fujimori, M. Fujisawa, T. Mori, I. Souma, and Y. Oka, Solid State Commun. **62**, 431 (1987).
[12]A. Franciosi, S. Chang, C. Caprile, R. Reifenberger, and U. Debska, J. Vac. Sci. Technol. A **3**, 926 (1985).
[13]R. Weidemann, B. Burmester, H.-E. Gumlich, Ch. Jung, T. Kleemann, T. Kreitler, A. Krost, H.-U. Middelmann, U. Becker, M. Kupsch, and S. Bernstorff, J. Cryst. Growth **101**, 916 (1990).
[14]L. Ley, M. Taniguchi, J. Ghijsen, R. L. Johnson, and A. Fujimori, Phys. Rev. B **35**, 2839 (1987).
[15]A. Franciosi, A. Wall, Y. Gao, J. H. Weaver, M.-H. Tsai, J. D. Dow, R. V. Kasowski, R. Reinfenberger, and F. Pool, Phys. Rev. B **40**, 12 009 (1989).
[16]A. Wall, A. Franciosi, D. W. Niles, R. Reifenberger, C. Quaresima, M. Capozi, and P. Perfetti, Phys. Rev. B **41**, 5969 (1990).
[17]M. Taniguchi, L. Ley, R. L. Johnson, J. Ghijsen, and M. Cardona, Phys. Rev. B **33**, 1206 (1986).
[18]A. Franciosi, C. Caprile, and R. Reinfenberg, Phys. Rev. B **31**, 8061 (1985).
[19]A. Wall, S. Chang, P. Philip, C. Caprile, A. Franciosi, R. Reifenberger, and F. Pool, J. Vac. Sci. Technol. A **5**, 2051 (1987).
[20]S.-H. Wei and A. Zunger, Phys. Rev. B **35**, 2340 (1987).
[21]K. C. Hass and H. Ehrenreich, Acta Phys. Pol. A **73**, 933 (1988).
[22]B. E. Larson, K. C. Hass, H. Ehrenreich, and H. E. Carlsson, Phys. Rev. B **37**, 4137 (1988).
[23]H. Xiaoguang and H. Meichun, J. Phys. Condens. Matter **1**, 5371 (1989).
[24]O. Gunnarsson, O. K. Andersen, O. Jepsen, and J. Zaanen, Phys. Rev. B **39**, 1708 (1989).
[25]J. W. Cooper, C. W. Clark, C. L. Cromer, T. B. Lucatorto, B. F. Sonntag, and F. S. Tomkins, Phys. Rev. B **35**, 3970 (1987).
[26]M. O. Krause, Th. A. Carlson, and A. Fahlman, Phys. Rev. A **30**, 1316 (1984).
[27]R. Bruhn, B. Sonntag, and H. W. Wolff, Phys. Lett. **69**, 9 (1978).
[28]J. M. Langer and H. Heinrich, Phys. Rev. Lett. **55**, 1414 (1985).
[29]A. Waag, Y. S. Wu, R. N. Bicknel-Tassius, and G. Landwehr, Appl. Phys. Lett. **54**, 2662 (1989).
[30]Y. C. Lu, R. S. Feigelson, and R. K. Route, J. Appl. Phys. **67**, 2583 (1990).
[31]P. John, T. Miller, T. C. Hsieh, A. P. Shapiro, A. L. Wachs, and T.-C. Chiang, Phys. Rev. B **34**, 6704 (1986).
[32]M. Pessa and O. Jylhä, Appl. Phys. Lett. **45**, 646 (1984).
[33]L. Ley, R. A. Pollak, F. R. McFeely, S. P. Kowalczyk, and D. A. Shirley, Phys. Rev. B **9**, 600 (1974).
[34]D. E. Eastman, W. D. Grobman, J. L. Freeouf, and M. Erbudak, Phys. Rev. B **9**, 3473 (1974).
[35]N. J. Shevchik, J. Tejeda, M. Cardona, and D. W. Langer, Phys. Status Solidi B **59**, 87 (1973).
[36]B. A. Bunker, W.-F. Pong, U. Debska, D. R. Yoder-Short, and J. K. Furdyna, in *Diluted Magnetic (Semimagnetic) Semiconductor* (Ref. 4), p. 237.
[37]A. Marbeuf, D. Ballutaud, R. Triboulet, H. Dexpert, P. Lagarde, and Y. Marfaing, J. Phys. Chem. Solids **50**, 975 (1989).
[38]The authors used the Fermi level of a thick-Au film deposited *a posteriori* onto the semiconductor surface as a binding energy reference.
[39]R. Denecke, J. Faul, L. Ley, J. Fraxadas, B. A. Orlowski, B. Kowalski, and K. Kopalko (unpublished).
[40]J. E. Bernard and A. Zunger, Phys. Rev. B **36**, 3199 (1987).
[41]S.-H. Wei and A. Zunger, Phys. Rev. Lett. **59**, 144 (1987).
[42]H. Asonen, J. Lilja, A. Vuoristo, M. Ishiko, and M. Pessa, Appl. Phys. Lett. **50**, 33 (1987).
[43]Least-squares fitting routine MINUET, available from the CERN computer center program library D516 (1976).
[44]The photoemission cross section for Zn 3*d* electrons is constant for photon energies between 42–60 eV, which we have checked by constant initial-state spectroscopy of the Zn 3*d* initial state. Also theoretical calculations by W. R. Johnson *et al.*, Phys. Rev. A **25**, 337 (1982), predict a plateau around 50 eV for the Zn 3*d* cross section in II-VI compounds.
[45]Band-structure calculations by N. E. Christensen *et al.*, J. Cryst. Growth **101**, 318 (1990), for the Zn 3*d* level in ZnSe show a dispersion of about 0.5 eV. However, to our knowledge no dispersion was obtained from angle-resolved photoemission experiments on Zn chalcogenides. Only on ZnTe a photon-energy dependence of the width of the Zn 3*d* emission were obtained by W. Wilke (Ph.D. thesis, Technical University, Berlin, 1989), but in this case the binding energy remains constant as well.
[46]L. C. Davis, Phys. Rev. B **25**, 2912 (1982).
[47]W. A. Harrison, *Electronic Structure and the Properties of Solids* (Freeman, San Francisco, 1980), pp. 253 and 519.
[48]Ch. G. van der Walle, K. Shahzad, and D. J. Olego, J. Vac. Sci. Technol. B **6**, 1350 (1980).
[49]A. Knack, H.-Ch. Mertins, and R. Weidemann (unpublished).
[50]A. Kisiel, J. Oleszkiewicz, M. Podgorny, G. Dalba, F. Rocca, and E. Burattini, J. Cryst. Growth **101**, 239 (1990).
[51]O. Gunnarsson, A. V. Postnikov, and O. K. Andersen, Phys. Rev. B **40**, 10 407 (1989).
[52]A. Wall, A. Raissanen, G. Haugstad, and A. Franciosi, Phys. Rev. B **44**, 8185 (1991).